A&A, 687, L17 (2024)
https://doi.org/10.1051/0004-6361/202450191

Astronomy & Astrophysics

LETTER TO THE EDITOR

Evidence for bipolar explosions in Type IIP supernovae

T. Nagao[1,2,3], K. Maeda[4], S. Mattila[1,5], H. Kuncarayakti[1,6], M. Kawabata[7], K. Taguchi[4], T. Nakaoka[8,9], A. Cikota[10], M. Bulla[11,12,13], S. S. Vasylyev[14,⋆], C. P. Gutiérrez[15,16], M. Yamanaka[17], K. Isogai[7,18], K. Uno[4], M. Ogawa[4], S. Inutsuka[4], M. Tsurumi[4], R. Imazawa[9], and K. S. Kawabata[8,9]

[1] Department of Physics and Astronomy, University of Turku, 20014 Turku, Finland
e-mail: t.nagao90@gmail.com
[2] Aalto University Metsähovi Radio Observatory, Metsähovintie 114, 02540 Kylmälä, Finland
[3] Aalto University Department of Electronics and Nanoengineering, PO BOX 15500, 00076 Aalto, Finland
[4] Department of Astronomy, Kyoto University, Kitashirakawa-Oiwake-cho, Sakyo-ku, Kyoto 606-8502, Japan
[5] School of Sciences, European University Cyprus, Diogenes Street, Engomi, 1516 Nicosia, Cyprus
[6] Finnish Centre for Astronomy with ESO (FINCA), University of Turku, Turku 20014, Finland
[7] Okayama Observatory, Kyoto University, 3037-5 Honjo, Kamogatacho, Asakuchi, Okayama 719-0232, Japan
[8] Hiroshima Astrophysical Science Center, Hiroshima University, Kagamiyama 1-3-1, Higashi-Hiroshima, Hiroshima 739-8526, Japan
[9] Department of Physical Science, Hiroshima University, Kagamiyama 1-3-1, Higashi-Hiroshima 739-8526, Japan
[10] Gemini Observatory/NSF's NOIRLab, Casilla 603, La Serena, Chile
[11] Department of Physics and Earth Science, University of Ferrara, Via Saragat 1, 44122 Ferrara, Italy
[12] INFN, Sezione di Ferrara, Via Saragat 1, 44122 Ferrara, Italy
[13] INAF, Osservatorio Astronomico d'Abruzzo, Via Mentore Maggini snc, 64100 Teramo, Italy
[14] Department of Astronomy, University of California, Berkeley, CA 94720-3411, USA
[15] Institut d'Estudis Espacials de Catalunya (IEEC), Edifici RDIT, Campus UPC, 08860 Castelldefels (Barcelona), Spain
[16] Institute of Space Sciences (ICE, CSIC), Campus UAB, Carrer de Can Magrans, s/n, 08193 Barcelona, Spain
[17] Amanogawa Galaxy Astronomy Research Center (AGARC), Graduate School of Science and Engineering, Kagoshima University, 1-21-35 Korimoto, Kagoshima, Kagoshima 890-0065, Japan
[18] Department of Multi-Disciplinary Sciences, Graduate School of Arts and Sciences, The University of Tokyo, 3-8-1 Komaba, Meguro, Tokyo 153-8902, Japan

Received 30 March 2024 / Accepted 19 June 2024

ABSTRACT

Aims. Recent observations of core-collapse supernovae (SNe) suggest aspherical explosions. Globally, aspherical structures in SN explosions are thought to encode information regarding the underlying explosion mechanism. However, the exact explosion geometries from the inner cores to the outer envelopes are poorly understood.
Methods. Here, we present photometric, spectroscopic, and polarimetric observations of the Type IIP SN 2021yja and discuss its explosion geometry in comparison to those of other Type IIP SNe that show large-scale aspherical structures in their hydrogen envelopes (SNe 2012aw, 2013ej and 2017gmr).
Results. During the plateau phase, SNe 2012aw and 2021yja exhibit high continuum polarization characterized by two components with perpendicular polarization angles. This behavior can be interpreted as being due to a bipolar explosion, where the SN ejecta is composed of a polar (energetic) component and an equatorial (bulk) component. In such a bipolar explosion, an aspherical axis created by the polar ejecta would dominate at early phases, while the perpendicular axis along the equatorial ejecta would emerge at late phases after the photosphere in the polar ejecta has receded. Our interpretation of the explosions in SNe 2012aw and 2021yja as bipolar is also supported by other observational properties, including the time evolution of the line velocities and the line shapes in the nebular spectra. The polarization of other Type IIP SNe that show large-scale aspherical structures in the hydrogen envelope (SNe 2013ej and 2017gmr) is also consistent with the bipolar-explosion scenario, although this is not conclusive.

Key words. techniques: polarimetric – supernovae: general – supernovae: individual

1. Introduction

Core-collapse supernovae (SNe) are catastrophic explosions due to the neutrino heating from a newly created protoneutron star after the collapse of the iron core (the neutrino-driven mechanism; e.g., Janka 2017) and characterize the deaths of massive stars. For a long time, it has been challenging to conduct first-principles simulations of SN explosions due to limitations in computational power. There are many complications and difficulties concerning nuclear and neutrino physics, the three-dimensional progenitor structures, and numerical challenges in the treatments of the transfer of the radiation and neutrinos and in general relativistic three-dimensional hydrodynamics calculations (e.g., Burrows & Vartanyan 2021). Recent advancements in computational power and the methodology for the calculations are beginning to allow successful simulations of SN explosions (e.g., Lentz et al. 2015; Melson et al. 2015; Radice et al. 2017;

⋆ Steven Nelson Graduate Fellow.

Vartanyan et al. 2018; Burrows et al. 2020). However, such successful explosions are limited to a small number of parameter sets of massive stars, and realistic SNe on a computer are still difficult to achieve for the majority of massive stars. Some key elements are therefore still missing in our understanding of SN explosions.

It has been suggested that some enhancements of multidimensional hydrodynamic instabilities, such as convective motion, the standing-accretion-shock instability (Blondin et al. 2003), and/or Rayleigh–Taylor instability, might play a crucial role because the multidimensional motions of the gas can increase the neutrino heating efficiency in the gain region (e.g., Burrows et al. 2020). Moreover, using state-of-the-art three-dimensional simulations based on the neutrino-driven mechanism, Burrows et al. (2024) demonstrated that successful explosions generally have global asymmetric structures and that this asymmetry is correlated with explosion energy. These findings are in agreement with recent observations of core-collapse SNe. Polarimetric observations have revealed large-scale aspherical structures in the ejecta of hydrogen-rich (Type II) SNe. Historically, a low level of polarization (~0.1%) has been measured during the plateau phase, followed by a rapid increase in continuum polarization at the beginning of the tail phase (e.g., Leonard et al. 2001, 2006; Chornock et al. 2010; Kumar et al. 2016). This polarimetric feature can be explained by an asymmetric helium core being revealed when the outer hydrogen envelope becomes optically thin as. Recently, Nagao et al. (2019) found an unprecedentedly highly extended aspherical explosion in Type II SN 2017gmr, indicated by an early rise in polarization even during the plateau phase. This shows that asymmetries are present not only in the helium core but also in a substantial portion of the hydrogen envelope. Furthermore, Nagao et al. (2024), using a large sample of SNe, discovered a correlation between the extension of the aspherical structures and the explosion energy, implying that the development of a global aspherical structure might be a key element in SN explosions. Such global aspherical structures in core-collapse SNe are also required by statistical analyses of line shapes in the nebular spectra of stripped-envelope SNe (e.g., Fang et al. 2024). This latter study demonstrates that the spatial distributions of the oxygen-burning ash and the unburnt oxygen follow the configurations of bipolar explosions. Moreover, the authors found that the degree of asphericity in such bipolar explosions increases as the progenitors become heavier.

In the present Letter, we analyze photometric, spectroscopic, and polarimetric observations of the Type IIP SN 2021yja and discuss its explosion geometry compared to those of other Type IIP SNe that show large-scale aspherical structures in the hydrogen envelope (SNe 2012aw, 2013ej and 2017gmr; Nagao et al. 2024). SN 2021yja was discovered by the Asteroid Terrestrial-impact Last Alert System (Smith et al. 2020) on 8.55 September 2021 UT (59465.55 MJD; Tonry et al. 2021). SN 2021yja is located in NGC 1325 (Galaxy Morphology: SA(s)bc; from NED[1]) at $z = 0.005307 \pm 0.000005$ and is receding with a velocity of $v_{\rm gal} = 1591 \pm 1\,{\rm km\,s^{-1}}$ (Springob et al. 2005). The object was not detected on 6.48 September 2021 UT (59463.48 MJD; Tonry et al. 2021). We adopt an explosion date of MJD 59464.40, estimated by Hosseinzadeh et al. (2022), which is approximately the midpoint between the last nondetection and the discovery dates. The object was classified as a Type II SN about 1 day after the discovery (59466.60 MJD; Pellegrino et al. 2021), and displayed prototypical observational properties for a Type IIP SN (e.g., Vasylyev et al. 2022; Hosseinzadeh et al. 2022). We adopted the Milky Way and host-galaxy reddening of $E(B-V)_{\rm MW} = 0.0191$ mag (Schlafly & Finkbeiner 2011) and $E(B-V)_{\rm host} = 0.085$ mag derived from the Na I D absorption lines by Hosseinzadeh et al. (2022), respectively, and thus a total reddening of $E(B-V) = 0.104$ mag. For the extinction correction, we adopt the extinction law by Fitzpatrick (1999). We adopt the distance and distance modulus for the SN of $23.4^{+5.4}_{-4.4}$ Mpc and $\mu = 31.85 \pm 0.45$ mag, respectively, which were derived using the Tully–Fisher estimate (Tully et al. 2016). In this work, we estimated the timing of the end of the plateau phase as the midpoint of the luminosity drop from the plateau phase to the tail phase following Nagao et al. (2024), by fitting the time evolution of the g-band light curve taken from Hosseinzadeh et al. (2022) with an artificial function (Eq. (1) in Nagao et al. 2024): $t = 59590.57$ MJD.

2. Observations

We performed photometric, spectroscopic, and polarimetric observations of the Type IIP SN 2021yja. The details of the photometric and spectroscopic observations are described in Appendices B and C. We obtained spectro- and imaging-polarimetry of the Type IIP SN 2021yja using the FOcal Reducer/low-dispersion Spectrograph 2 (hereafter FORS2) mounted at the Cassegrain focus of the Very Large Telescope (VLT) UT1 telescope at the Paranal observatory and the Alhambra Faint Object Spectrograph and Camera (ALFOSC) mounted on the 2.56 m Nordic Optical Telescope (NOT) at the Roque de los Muchachos Observatory. The observing logs are shown in Tables A.1 and A.2. We note that spectropolarimetric observations of SN 2021yja were also conducted and reported by Vasylyev et al. (2024). Here, our polarimetric data cover later epochs.

The spectropolarimetric observations and their analysis are similar to those reported in Nagao et al. (2023). We observed SN 2021yja using the low-resolution G300V grism and a half-wave retarder plate (HWP) with the optimal set of HWP angles of 0°, 22.5°, 45°, and 67.5°. The raw data were reduced with IRAF (Tody 1986, 1993) using standard methods as described, for example, in Patat & Romaniello (2006). From the reduced object frames, we extracted the ordinary and extraordinary beams of the SN with a fixed aperture size of 10 pixels, and rebinned the extracted spectra to 50 Angstrom bins to allow a better signal-to-noise ratio. We also corrected the observations for HWP zero-point angle chromatism using tabulated values for the zero-angle given in the FORS2 user manual[2]. The wavelength scale was corrected to the rest frame using the host-galaxy redshift. In order to derive the continuum polarization from the spectropolarimetric data, we used the wavelength ranges between 6800 and 7200 Å and between 7820 and 8140 Å following (Nagao et al. 2024). For the imaging polarimetry, the same instrumental setup was adopted, using a narrow-band filter (FILT_815_13) with the VLT and two broad band filters (V and R) with the NOT instead of the grism in the optical path. We applied bias subtraction and flat-field correction to all the frames and then performed aperture photometry on each detected source. For the aperture photometry, we used an aperture size that is twice as large as the full width at half maximum (FWHM) of the point spread function of the ordinary beam and a background region whose inner and outer radii are twice and four times as large as the FWHM, respectively. Based on these

[1] NASA/IPAC Extragalactic Database.

[2] http://www.eso.org/sci/facilities/paranal/instruments/fors/doc/VLT-MAN-ESO-13100-1543_P07.pdf

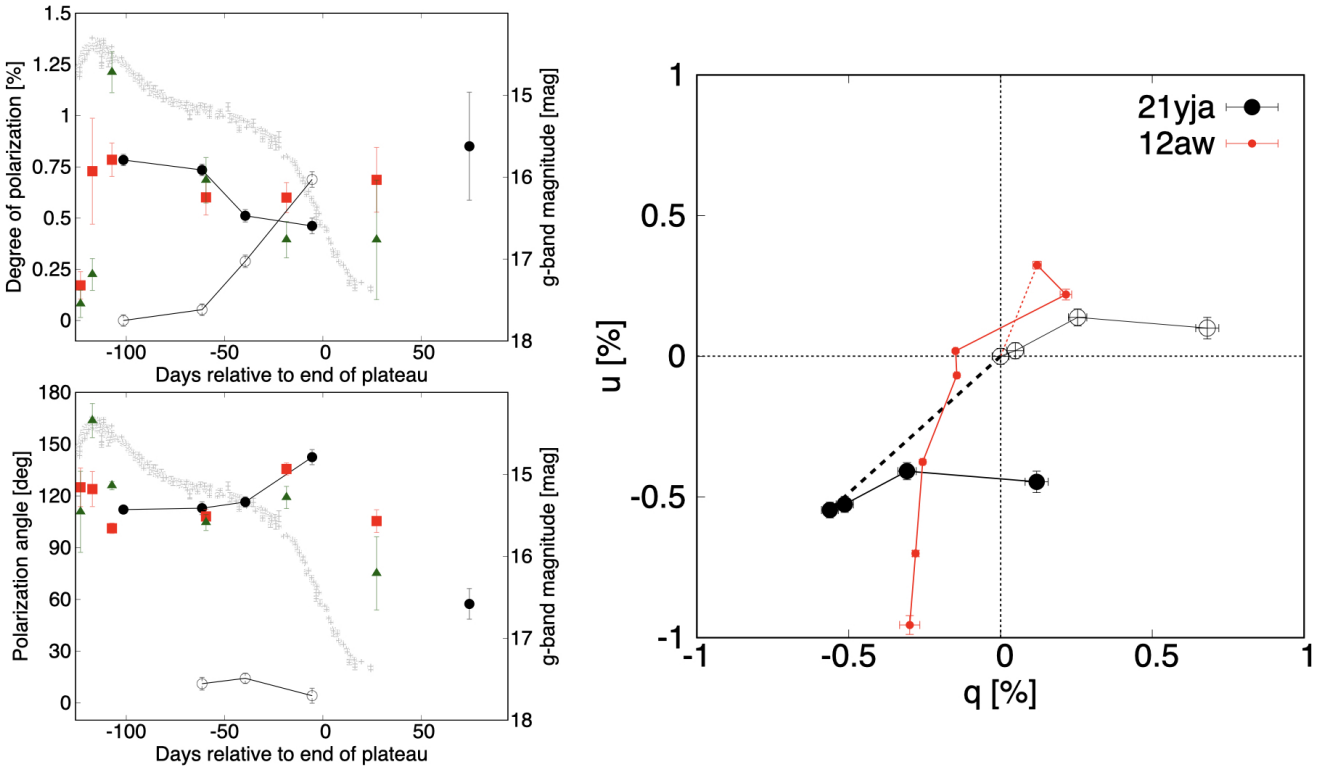

Fig. 1. Time evolution of the continuum polarization of SN 2021yja. Left panel: Polarization degree and angle of SN 2021yja. The filled black circles connected by a solid line show the continuum polarization derived from the polarization spectra, while the filled green triangles and red squares show the values from the *V*- and *R*-band imaging polarimetry. The open black circles represent only the second component of the continuum polarization. The gray crosses trace the *g*-band light curve of SN 2021yja taken from Hosseinzadeh et al. (2022). Right panel: Time evolution of the continuum polarization in the q-u plane compared to that of SN 2012aw. The first epochs are indicated with dotted lines. The open black circles are the same in the left panels, representing only the second component of the continuum polarization.

values, we calculated the Stokes parameters, the linear polarization degree, and the polarization angle. When calculating the polarization degrees, we subtracted the polarization bias, following Wang et al. (1997). As the polarization degrees on the Hα emission line – where the intrinsic polarization is supposed to be depolarized and thus the interstellar polarization (ISP) should be dominant (e.g., Nagao et al. 2023) – are close to zero, we assume that the ISP in SN 2021yja is negligibly small, which is also adopted by Vasylyev et al. (2024).

3. Results and discussion

Figure 1 shows the continuum polarization of SN 2021yja derived from spectropolarimetry and from the narrow and broad-band polarization. As also seen in Vasylyev et al. (2024), SN 2021yja shows a distinct evolution of the continuum polarization compared with the majority of other Type IIP SNe. Most Type IIP SNe show low polarization degrees at early phases and a sudden rise to ∼1% at a certain point in the plateau phase, with a constant polarization angle (see, e.g., Nagao et al. 2024). In contrast, SN 2021yja shows a high degree of polarization (∼0.8%) at early phases and a decline in polarization degree with time as well as a gradual change of the polarization angle. This implies multiaxial structures in the hydrogen envelope, whose relative contributions to the polarization evolve with time. The *V*- and *R*-band data are generally consistent with the continuum polarization estimated from the polarization spectra, even though they should be affected by line depolarization or polarization (see the polarization spectra in Appendix A) and have larger errors. Hereafter, when discussing the continuum polarization of SN 2021yja, we only use the values derived from the polarization spectra. We note that the polarization angles in the tail phase estimated from the narrow-band, *V*-, and *R*-band imaging polarimetry are not stable and thus might indeed be affected by line polarization. In the tail phase, the line polarization can dominate over the continuum polarization (see, e.g., the cases of SNe 2017gmr and 2013ej; Nagao et al. 2019, 2021). As we do not have spectropolarimetry for the tail phase, we do not further discuss the polarization in the tail phase in this Letter.

We adopt the continuum polarization derived from the first-epoch spectropolarimetric data as the "first component" (P = 0.78%, θ = 112.1°). We then subtract the first component from the original continuum polarization. The remaining polarization shows a relatively constant polarization angle ($\theta \sim 15°$), which we refer to as the "second component". This means that the continuum polarization during the plateau phase can be explained by these two components. We note that, if we assume that the polarization degree of the first component with θ = 112.1° is not constant but variable in time, the remaining polarization after the subtraction of the first component from the original polarization still shows time-variable polarization angles. Therefore, in order to remove the time variability of the polarization angle of the remaining polarization, at least two additional polarization sources are required. Consequently, we need at least three components of the polarization in total as the origin of the continuum polarization. In addition, any of these components would not show typical time evolution of the polarization degrees as in other Type IIP SNe (Nagao et al. 2024). The difference between

the polarizatiton angles of these components is ~95°. In the q-u plane, the data points of the second component (open black circles) are clearly located in almost the opposite direction relative to the first component (dotted line) toward the origin of the q-u plane, demonstrating that the axes of the aspherical structures implied by the first and second components are almost perpendicular (Fig. 1).

In the literature, several other Type II SNe have been reported to clearly show time-variable polarization angles in their polarization, implying multiaxis structures in the ejecta (SNe 2012aw, 2013ej and 2023ixf; Nagao et al. 2021, 2024; Vasylyev et al. 2024). SN 2023ixf showed high continuum polarization with a different polarization angle from that seen in later phases within just a few days following the explosion, which coincides with the existence of highly ionized "flash" features in the spectra (Vasylyev et al. 2022). As the flash features are created by highly ionized gas in confined circumstellar material (CSM) due to high-energy photons created in an interaction between the SN ejecta and the CSM (e.g., Boian & Groh 2020), we conclude that this short-lived component of the polarization reflects the aspherical structure not of the SN ejecta but of the confined CSM (Vasylyev et al. 2024). In the case of SN 2013ej, the evolution of the polarization angle occurred over the greater part of the plateau phase (Nagao et al. 2021). At the same time, the SN showed observational signs of a major CSM interaction at least during the first several tens of days (e.g., Bose et al. 2015). This evolution of the polarization is understood as a manifestation of the change in the contributions from two different aspherical structures, one originating from an aspherical CSM interaction and the other from the aspherical SN ejecta. On the contrary, SNe 2012aw and 2021yja do not show observational features from a strong CSM interaction able to change the global properties of the SN ejecta, although a weak CSM interaction is predicted (e.g., Bose et al. 2013; Hosseinzadeh et al. 2022; Vasylyev et al. 2022). The low degree of the early-phase broadband polarization in SN 2021yja also disagrees with the scenario of a major spherical CSM interaction as in the case of SN 2013ej. Furthermore, the change in the polarization angle between the first and second components in the cases of SNe 2012aw and 2021yja is close to ~90°, demonstrating that the axes of these two components are close to perpendicular, which is different from the case of SN 2013ej (~20°; Nagao et al. 2021). If the first and second components originate from an aspherical CSM interaction and aspherical SN ejecta, respectively (as in the case of SN 2013ej), the angle change should be random due to the random orientation between the CSM structure and the aspherical SN explosion; unless there is some mechanism to create a common preferential axis for the mass loss and the SN explosion.

We propose that this is evidence of a two-component ejecta driven by a bipolar explosion (a collimated energetic component and a canonical bulk SN component), as invoked by Nagao et al. (2024) in order to explain the polarization in SN 2012aw. We consider a similar situation to the bipolar ejecta model proposed by Kaplan & Soker (2020). A schematic picture of this scenario is shown in Fig. 2. If an energy injection is stronger in the polar directions than in the equatorial directions, the ejecta in the polar direction (the energetic component) would create a larger photosphere than that in the equatorial directions (the bulk component) at early phases (Phase 1). As the withdrawal of the photosphere happens earlier in the polar directions than in the equatorial directions, the size of the photosphere in the energetic component becomes smaller than that in the bulk component late in the plateau phase (Phase 2). This transition from Phase 1 to Phase 2 creates the 90° change in the angle of the axis of the aspherical

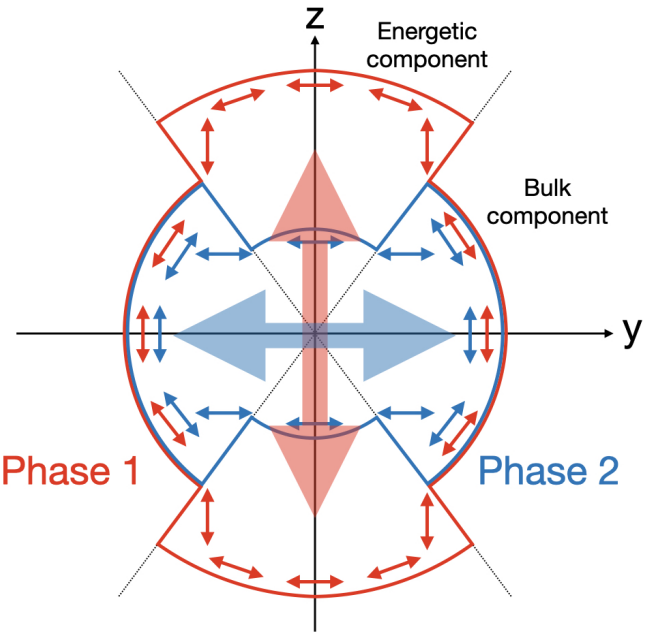

Fig. 2. Schematic presentation of the continuum polarization in SN2021yja (observer's view) created by a bipolar explosion. At early phases, the photosphere is extended vertically due to the energetic ejecta component, which creates the first vertical polarization component (Phase 1). Then, the shape of the photosphere is crushed horizontally because of the withdrawal of the photosphere in the energetic component, which creates the second horizontal polarization component (Phase 2). This explains the rotation of the observed polarization angle. The polarization vectors of important individual photons from the photosphere are indicated with small arrows. The large arrows show the net polarization vectors of all the photons.

structures. Such a morphology change has also been predicted by past radiative transfer calculations in a bipolar explosion (e.g., Maeda et al. 2006; Dessart et al. 2024).

The relative strength of the first and second components and their time evolution should depend on the ejecta parameters (mass, energy, and collimation degree) for the polar and equatorial directions and on the viewing angle. In particular, the timing of the transition from Phase 1 to Phase 2 should not strongly depend on the viewing angle, but on the explosion parameters and the degree of the collimation of the energetic component. For example, if we assume that the explosion properties are independent for these perpendicular directions and that only the inputted specific explosion energy to these components is different, the timing of the transition from Phase 1 to Phase 2 can be roughly estimated from the relative explosion energy using the scaling relation in a simple one-zone model of homogeneously expanding gas with radiative diffusion proposed by Kasen & Woosley (2009): $t_{\rm sn} \propto E^{-1/6}$. In the case where the energetic component has ten times greater specific energy than the bulk component, this transition will happen at 70% of the plateau length of the bulk component, although it should be a relatively smooth transition in reality. Observations show that the timing of this phase transition in SNe 2012aw is different from that in 2021yja: there was an earlier transition in the case of SN 2012aw compared to SN 2021yja. This might imply that there is diversity in the bipolar structures in Type IIP SNe. We also note that, as the relative strength of the two components depends on the viewing angle, the different viewing angles might also contribute to the different timing of the exchange of these two components to some extent.

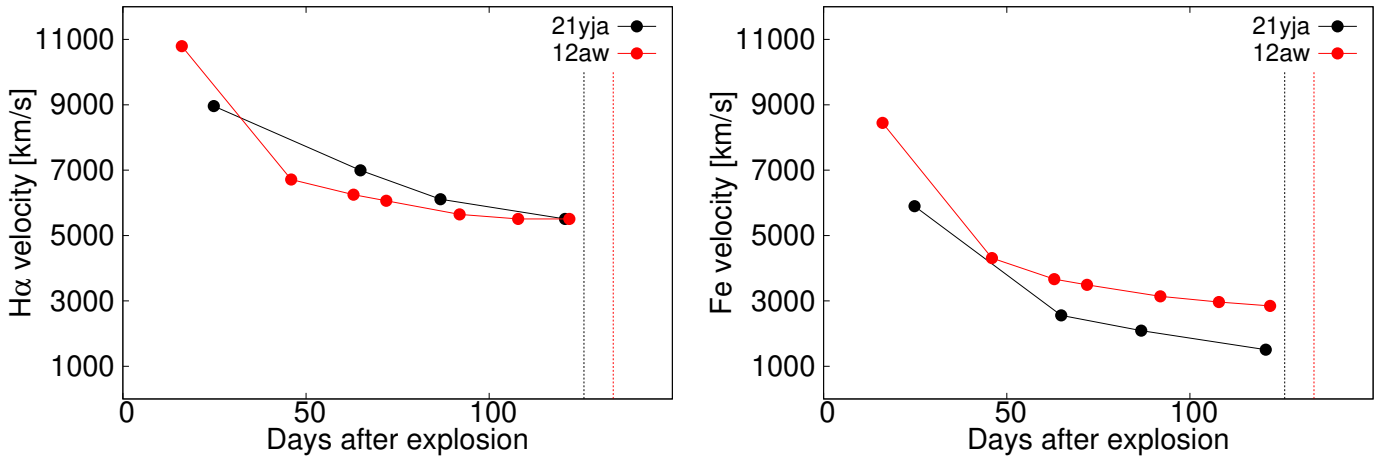

Fig. 3. Time evolution of the Hα and Fe II velocities derived from the absorption minima of the respective lines. The vertical dotted lines indicate the timings of the end of the plateau phase.

There may exist other mechanisms able to create such a bipolar structure before the explosion; for example, by some unknown aspherical energy injection just before the explosion or by extremely rapid rotation. However, SN 2021yja shows low polarization at very early phases ($\lesssim$0.2% at Phase +2.78), which might suggest that the outermost layer of the ejecta is relatively spherical. Therefore, this bipolar structure in SN 2021yja might not be due to the inherent aspherical structure in the progenitor star but a bipolar explosion. We note that the low polarization at early phases might be achieved due to the high optical depth for electron scattering in the outermost layer (e.g., Dessart & Hillier 2011), even if the progenitor originally has an aspherically extended envelope. This effect depends on the density distribution in the extended envelope and should be quantitatively tested.

The other Type IIP SN that showed large-scale aspherical structures in the hydrogen envelope (SN 2017gmr Nagao et al. 2019) did not show the two-component polarization, which is different from the cases of SNe 2012aw and 2021yja. However, the earliest polarimetric observation of SN 2017gmr was conducted 45.40 days after the first detection, and thus the first component might have already been covered by the second component (see the case of SN 2012aw in Nagao et al. 2024). Alternatively, the first component might be weak due to the viewing angle. So far, all the Type IIP SNe that show global aspherical structures in the hydrogen envelope (energetic Type II SNe Nagao et al. 2024) are consistent with the bipolar-explosion scenario. It is important to increase the sample size in order to probe the diversity in bipolar explosions.

The interpretation of SNe 2012aw and 2021yja as bipolar explosions is also supported by other observational properties. The general photometric and spectroscopic properties of SNe 2012aw and 2021yja are relatively similar (e.g., plateau luminosity, plateau length, and the velocity evolution of the Hα line; see Appendices B and C), implying that the basic parameters of the SN ejecta are relatively similar. However, they show a different feature in the velocity evolution of the Fe II λ5169 line, which is often used as a tracer of the velocity of the photosphere. At early phases, both SNe show a similar velocity evolution of the Fe II line, while SN 2021yja shows slower velocities than SN 2012aw at later phases (Fig. 3). This observational property might be explained by the different viewing angles toward relatively similar bipolar explosions. The viewing angle of SN 2021yja is closer to the polar direction compared to that of

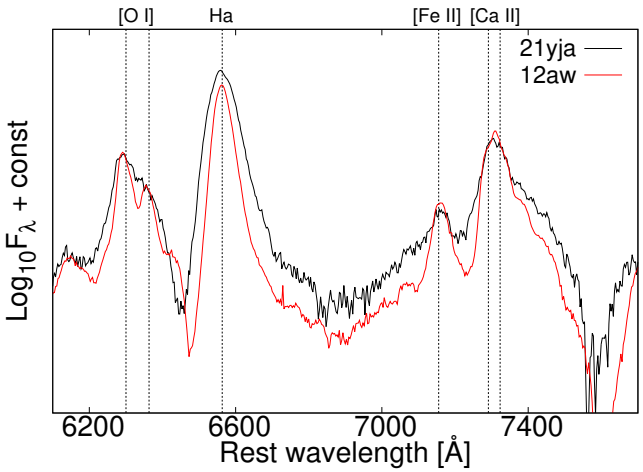

Fig. 4. ALFOSC/NOT spectrum of SN 2021yja at 352.82 days after the explosion compared to the spectrum of SN 2012aw obtained with the same instrument and telescope (ALFOSC/NOT) at +369 days after the explosion (Jerkstrand et al. 2014). Wavelengths of prominent lines are indicated with vertical dashed lines.

SN 2012aw. Thus, the drop in the Fe II velocity might be related to the withdrawal of the photosphere in the energetic component of the ejecta, that is, the transition from Phase 1 to Phase 2. This might also be the reason why the relative strength of the first polarization component compared to the second component in SN 2021yja is larger than that in SN 2012aw.

Nebular spectroscopy is also a powerful tool for studying the geometry of the SN ejecta, especially for the inner parts (e.g., Maeda et al. 2008; Taubenberger et al. 2009; Fang et al. 2024), while polarimetry during the plateau phase provides information on the structure of the hydrogen envelope, as discussed above. Figure 4 shows a part of the nebular spectra of SNe 2021yja and 2012aw taken with the ALFOSC/NOT (see Appendix C for details). SN 2021yja shows a broader [Fe II] λ 7155 line than that observed in SN 2012aw, although the Fe II velocity during the plateau phase in SN 2021yja was slower than that seen in SN 2012aw. In addition, the [Ca II] $\lambda\lambda$ 7291,7323 lines are wider than those seen in SN 2012aw, while their [O I] $\lambda\lambda$ 6300,6363 lines are similar. These properties might also be explained by a scenario with the viewing angle effects of a bipolar explosion: The viewing angle of SN 2021yja is closer to the polar direction

compared to that of SN 2012aw. As the energetic ejecta component creates more burning ash (Fe and Ca) than the bulk component, the relative line widths of the iron and calcium lines to the oxygen line can be larger if the viewing angle is closer to the polar direction. This interpretation is consistent with the properties of the polarization and the line velocities. This also suggests that the aspherical structure of the hydrogen envelope extends into the inner core, maintaining its shape. This provides strong evidence in favor of the bipolar-explosion scenario, disfavoring the possibility of the CSM interaction scenario.

Acknowledgements. This work is partly based on observations collected at the European Organisation for Astronomical Research in the Southern Hemisphere (ESO) under programmes 108.228k.001 and 108.228k.002. This work is partly based on observations made under program IDs P63-016, P64-023 and P65-005 with the Nordic Optical Telescope, owned in collaboration by the University of Turku and Aarhus University, and operated jointly by Aarhus University, the University of Turku and the University of Oslo, representing Denmark, Finland and Norway, the University of Iceland and Stockholm University at the Observatorio del Roque de los Muchachos, La Palma, Spain, of the Instituto de Astrofisica de Canarias. The data from the Seimei and Kanata telescopes were taken under the KASTOR (Kanata And Seimei Transient Observation Regime) project (Seimei program IDs: 21B-N-CT09, 21B-K-0004, 21B-K-0011, 22A-K-0004, 22A-O-0003, 22B-N-CT10, 22B-K-0003). The Seimei telescope at the Okayama Observatory is jointly operated by Kyoto University and the Astronomical Observatory of Japan (NAOJ), with assistance provided by the Optical and Near-Infrared Astronomy Inter-University Cooperation Program. This research was made possible through the use of the AAVSO Photometric All-Sky Survey (APASS), funded by the Robert Martin Ayers Sciences Fund and NSF AST-1412587. T.N. acknowledges support from the Research Council of Finland projects 324504, 328898 and 353019. K.M. acknowledges support from the Japan Society for the Promotion of Science (JSPS) KAKENHI grant (JP20H00174 and JP24H01810) and by the JSPS Open Partnership Bilateral Joint Research Project between Japan and Finland (JPJSBP120229923). S.M. was funded by the Research Council of Finland project 350458. H.K. was funded by the Research Council of Finland projects 324504, 328898, and 353019. C.P.G. acknowledges financial support from the Secretary of Universities and Research (Government of Catalonia) and by the Horizon 2020 Research and Innovation Programme of the European Union under the Marie Skłodowska-Curie and the Beatriu de Pinós 2021 BP 00168 programme, from the Spanish Ministerio de Ciencia e Innovación (MCIN) and the Agencia Estatal de Investigación (AEI) 10.13039/501100011033 under the PID2020-115253GA-I00 HOSTFLOWS project, and the program Unidad de Excelencia María de Maeztu CEX2020-001058-M. This work was supported by JST, the establishment of university fellowships towards the creation of science technology innovation, Grant Number JPMJFS2129.

References

Blondin, J. M., Mezzacappa, A., & DeMarino, C. 2003, ApJ, 584, 971
Boian, I., & Groh, J. H. 2020, MNRAS, 496, 1325
Bose, S., Kumar, B., Sutaria, F., et al. 2013, MNRAS, 433, 1871
Bose, S., Sutaria, F., Kumar, B., et al. 2015, ApJ, 806, 160
Brown, P. J., Breeveld, A. A., Holland, S., Kuin, P., & Pritchard, T. 2014, Ap&SS, 354, 89
Burrows, A., & Vartanyan, D. 2021, Nature, 589, 29
Burrows, A., Radice, D., Vartanyan, D., et al. 2020, MNRAS, 491, 2715
Burrows, A., Wang, T., & Vartanyan, D. 2024, ApJ, 964, L16
Chornock, R., Filippenko, A. V., Li, W., & Silverman, J. M. 2010, ApJ, 713, 1363
Dall'Ora, M., Botticella, M. T., Pumo, M. L., et al. 2014, ApJ, 787, 139
Dessart, L., & Hillier, D. J. 2011, MNRAS, 415, 3497
Dessart, L., Hillier, D. J., & Leonard, D. C. 2024, A&A, 684, A16
Fang, Q., Maeda, K., Kuncarayakti, H., & Nagao, T. 2024, Nat. Astron., 8, 111
Fitzpatrick, E. L. 1999, PASP, 111, 63
Henden, A. A., Levine, S. E., Terrell, D., Smith, T. C., & Welch, D. 2012, JAAVSO, 40, 430
Hosseinzadeh, G., Kilpatrick, C. D., Dong, Y., et al. 2022, ApJ, 935, 31
Janka, H. T. 2017, in Handbook of Supernovae, eds. A. W. Alsabti, & P. Murdin, 1095
Jerkstrand, A., Smartt, S. J., Fraser, M., et al. 2014, MNRAS, 439, 3694
Jester, S., Schneider, D. P., Richards, G. T., et al. 2005, AJ, 130, 873
Kaplan, N., & Soker, N. 2020, MNRAS, 494, 5909
Kasen, D., & Woosley, S. E. 2009, ApJ, 703, 2205
Kawabata, K. S., Nagae, O., Chiyonobu, S., et al. 2008, in Ground-based and Airborne Instrumentation for Astronomy II, eds. I. S. McLean & M. M. Casali, SPIE Conf. Ser., 7014, 70144L
Kumar, B., Pandey, S. B., Eswaraiah, C., & Kawabata, K. S. 2016, MNRAS, 456, 3157
Kurita, M., Kino, M., Iwamuro, F., et al. 2020, PASJ, 72, 48
Lentz, E. J., Bruenn, S. W., Hix, W. R., et al. 2015, ApJ, 807, L31
Leonard, D. C., Filippenko, A. V., Ardila, D. R., & Brotherton, M. S. 2001, ApJ, 553, 861
Leonard, D. C., Filippenko, A. V., Ganeshalingam, M., et al. 2006, Nature, 440, 505
Maeda, K., Mazzali, P. A., & Nomoto, K. 2006, ApJ, 645, 1331
Maeda, K., Kawabata, K., Mazzali, P. A., et al. 2008, Science, 319, 1220
Matsubayashi, K., Ohta, K., Iwamuro, F., et al. 2019, PASJ, 71, 102
Melson, T., Janka, H.-T., & Marek, A. 2015, ApJ, 801, L24
Munari, U., Henden, A., Belligoli, R., et al. 2013, New Astron., 20, 30
Nagao, T., Cikota, A., Patat, F., et al. 2019, MNRAS, 489, L69
Nagao, T., Patat, F., Taubenberger, S., et al. 2021, MNRAS, 505, 3664
Nagao, T., Mattila, S., Kotak, R., & Kuncarayakti, H. 2023, A&A, 678, A43
Nagao, T., Patat, F., Cikota, A., et al. 2024, A&A, 681, A11
Patat, F., & Romaniello, M. 2006, PASP, 118, 146
Pellegrino, C., Burke, J., Hiramatsu, D., et al. 2021, TNS Classif. Rep., 2021-3115, 1
Radice, D., Burrows, A., Vartanyan, D., Skinner, M. A., & Dolence, J. C. 2017, ApJ, 850, 43
Schlafly, E. F., & Finkbeiner, D. P. 2011, ApJ, 737, 103
Smith, K. W., Smartt, S. J., Young, D. R., et al. 2020, PASP, 132, 085002
Springob, C. M., Haynes, M. P., Giovanelli, R., & Kent, B. R. 2005, ApJS, 160, 149
Stetson, P. B. 1987, PASP, 99, 191
Taubenberger, S., Valenti, S., Benetti, S., et al. 2009, MNRAS, 397, 677
Tody, D. 1986, in Instrumentation in Astronomy VI, ed. D. L. Crawford, SPIE Conf. Ser., 627, 733
Tody, D. 1993, in Astronomical Data Analysis Software and Systems II, eds. R. J. Hanisch, R. J. V. Brissenden, & J. Barnes, ASP Conf. Ser., 52, 173
Tonry, J., Denneau, L., Heinze, A., et al. 2021, TNSTR, 2021-3093, 1
Tully, R. B., Courtois, H. M., & Sorce, J. G. 2016, AJ, 152, 50
Vartanyan, D., Burrows, A., Radice, D., Skinner, M. A., & Dolence, J. 2018, MNRAS, 477, 3091
Vasylyev, S. S., Filippenko, A. V., Vogl, C., et al. 2022, ApJ, 934, 134
Vasylyev, S. S., Yang, Y., Patra, K. C., et al. 2024, MNRAS, 527, 3106
Wang, L., Wheeler, J. C., & Höflich, P. 1997, ApJ, 476, L27

Appendix A: Polarimetry

The observing logs for the spectro- and imaging polarimetry of SN 2021yja are presented in Tables A.1 and A.2. The full polarization spectra are shown in Figure A.1 and A.2.

Table A.1. Log and measurements of the spectropolarimetric observations of SN 2021yja.

Date (UT)	MJD (days)	Phase[a] (days)	Days from explosion[b] (days)	Exp. time (seconds)	Pol. degree[c] (%)	Pol. angle[c] (degrees)	Telescope
2021 – 10 – 02.24	59489.24	–101.33	+24.84	4 × 300	0.78(0.00) ± 0.03	112.1(–) ± 1.4	VLT
2021 – 11 – 11.26	59529.26	–61.31	+64.86	4 × 300	0.74(0.05) ± 0.03	112.9(11.1) ± 3.7	VLT
2021 – 12 – 03.09	59551.09	–39.48	+86.69	4 × 300	0.51(0.29) ± 0.03	116.5(14.3) ± 3.0	VLT
2022 – 01 – 06.10	59585.10	–5.47	+120.70	4 × 300	0.46(0.69) ± 0.04	142.5(4.2) ± 4.4	VLT

Notes. [a]Relative to t_0 = 59590.57 (MJD), which is the estimated time of the end of the plateau phase. [b]Relative to t = 59464.40 (MJD), which is the estimated explosion time. [c]Continuum polarization degree and angle. The values in brackets for the polarization degree and angle refer to the continuum polarization after subtraction of the first component. The errors of the polarization degrees and angles represent the photon shot noise.

Table A.2. Log and measurements of the imaging-polarimetric observations of SN 2021yja.

Date (UT)	MJD (days)	Phase (days)	Days from explosion (days)	Exp. time (seconds)	Pol. degree (%)	Pol. angle (degrees)	Filter	Telescope
2021-09-10.18	59467.18	-123.39	+2.78	4 × 40	0.08 ± 0.07	110.8 ± 23.5	V	NOT
				4 × 40	0.17 ± 0.07	125.0 ± 11.2	R	
2021-09-16.22	59473.22	-117.35	+8.82	4 × 30	0.22 ± 0.08	163.6 ± 9.9	V	NOT
				4 × 30	0.73 ± 0.26	124.0 ± 10.2	R	
2021-09-26.16	59483.16	-107.41	+18.76	4 × 30	1.21 ± 0.10	125.9 ± 2.4	V	NOT
				4 × 30	0.78 ± 0.08	101.2 ± 3.0	R	
2021-11-13.01	59531.01	-59.56	+66.61	4 × 30	0.68 ± 0.11	104.6 ± 4.6	V	NOT
				4 × 30	0.60 ± 0.09	108.1 ± 4.1	R	
2021-12-23.96	59571.96	-18.61	+107.56	4 × 40	0.39 ± 0.09	119.1 ± 6.4	V	NOT
				4 × 30	0.60 ± 0.07	135.6 ± 3.5	R	
2022-02-07.83	59617.83	+27.26	+153.43	4 × 100	0.39 ± 0.29	75.1 ± 21.2	V	NOT
				4 × 80	0.69 ± 0.16	105.4 ± 6.6	R	
2022 – 03 – 27.01	59665.01	+74.44	+200.61	4 × 300	0.85 ± 0.26	57.4 ± 8.9	FILT_815_13	VLT

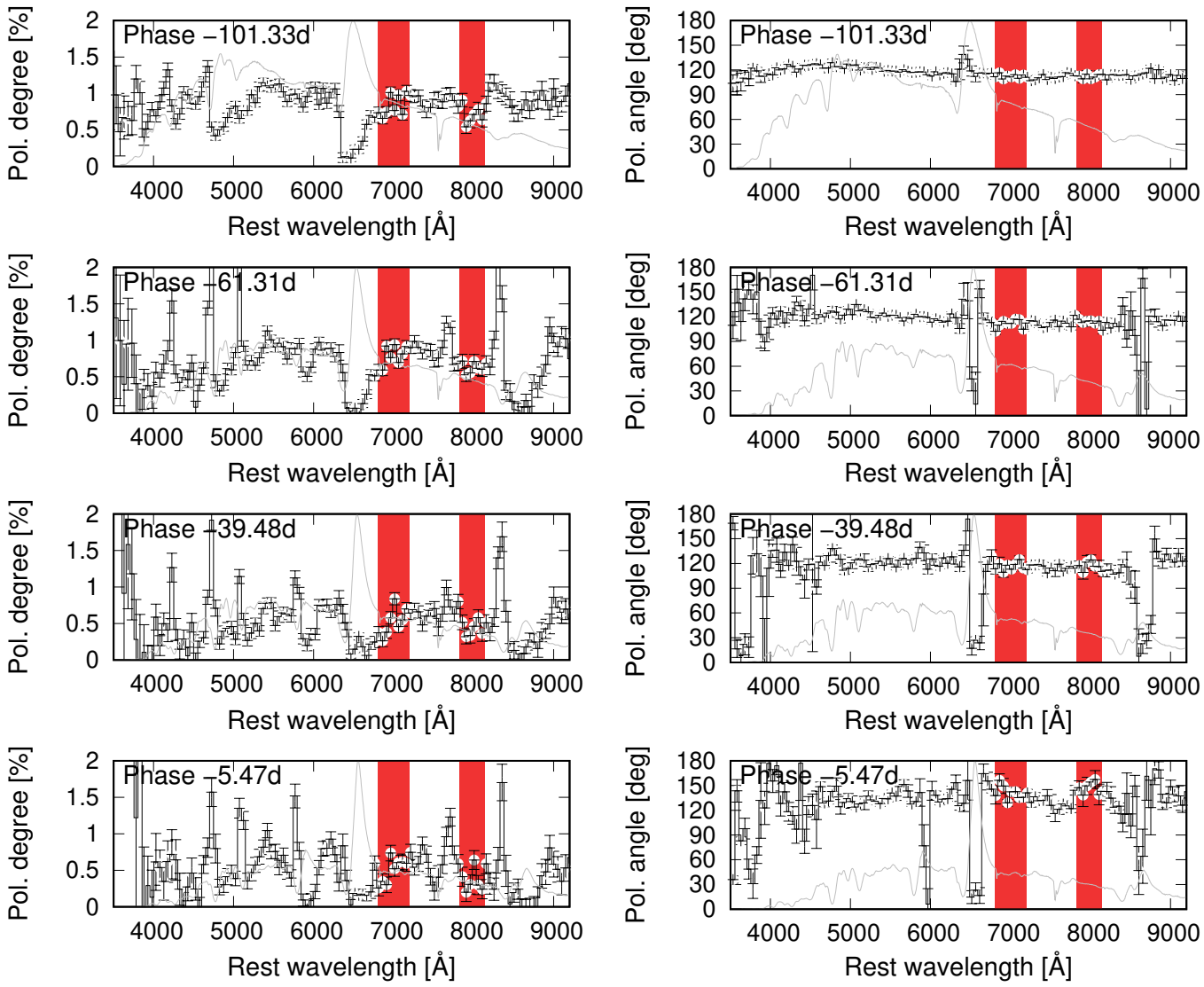

Fig. A.1. Polarization degree (left) and angle (right) of SN 2021yja. The red hatching shows the adopted wavelength range for the estimation of continuum polarization. The grey lines in the background of each plot are the unbinned flux spectra at the corresponding epochs.

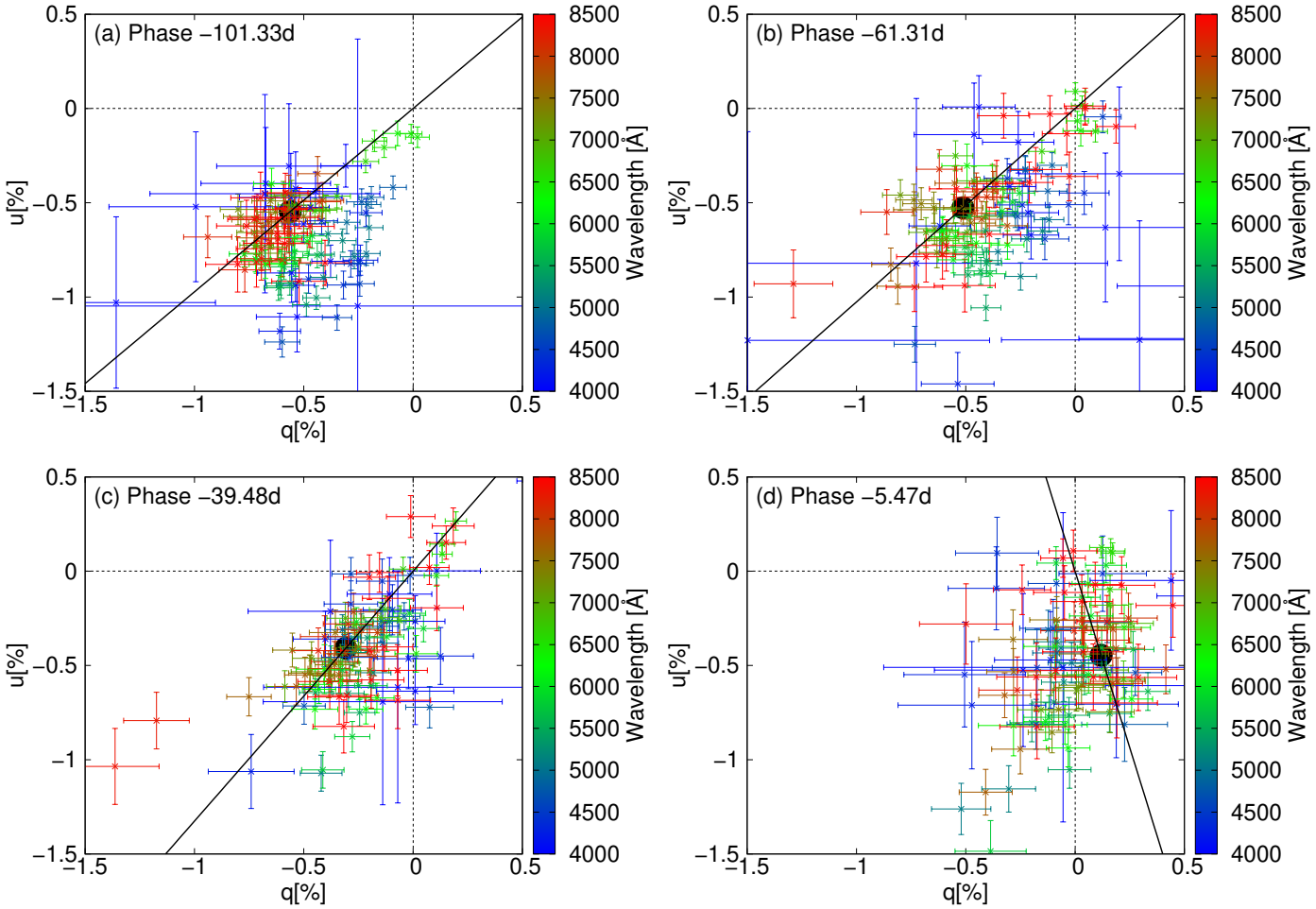

Fig. A.2. Spectropolarimetric data in the q-u plane. The estimated continuum polarization and its angle are shown with black points and lines, respectively.

Appendix B: Photometry

We obtained *B*-, *V*−, *R*- and *I*-band photometry of SN 2021yja using the Hiroshima One-shot Wide-field Polarimeter (HOWPol; Kawabata et al. 2008) mounted on the 1.5-m Kanata telescope at the Higashi-Hiroshima Observatory in Japan. We performed the point spread function (PSF) photometry using the DAOPHOT package (Stetson 1987) as a part of IRAF. Since the host galaxy at the SN position is faint, we did not subtract the template images for the photometry. The magnitudes of the local comparison stars were obtained from the AAVSO Photometric All-Sky Survey (APASS; Henden et al. 2012). We estimated the *R*- and *I*-band magnitudes of the comparison stars from the Sloan magnitudes using the relations in Jester et al. (2005). The results of photometry are provided in Table B.1 and Figures B.1 and B.2.

Table B.1. Log of the photometric observations of SN 2021yja and photometric measurements (Vega magnitudes).

MJD (days)	Days from explosion (days)	B (mag)	V (mag)	R (mag)	I (mag)
59488.75	+24.35	15.11 ± 0.03	14.70 ± 0.03	14.37 ± 0.03	14.27 ± 0.02
59489.72	+25.32	15.18 ± 0.02	14.66 ± 0.02	14.34 ± 0.02	14.23 ± 0.02
59490.78	+26.38	15.26 ± 0.02	14.67 ± 0.03	14.38 ± 0.02	14.25 ± 0.03
59492.75	+28.35	15.29 ± 0.02	14.69 ± 0.02	14.36 ± 0.02	14.21 ± 0.02
59494.71	+30.31	15.35 ± 0.02	14.72 ± 0.02	14.35 ± 0.02	14.22 ± 0.02
59495.79	+31.39	15.46 ± 0.02	14.79 ± 0.03	14.42 ± 0.02	14.24 ± 0.03
59496.68	+32.28	15.38 ± 0.02	14.73 ± 0.02	14.36 ± 0.02	14.23 ± 0.03
59501.77	+37.37	15.62 ± 0.02	14.82 ± 0.02	14.44 ± 0.02	14.27 ± 0.02
59512.74	+48.34	15.88 ± 0.02	14.90 ± 0.03	14.48 ± 0.02	14.31 ± 0.02
59536.62	+72.22	16.06 ± 0.03	14.98 ± 0.02	14.49 ± 0.02	14.27 ± 0.02
59545.65	+81.25	16.09 ± 0.02	15.00 ± 0.02	14.49 ± 0.02	14.28 ± 0.02
59561.55	+97.15	16.36 ± 0.02	15.20 ± 0.02	14.59 ± 0.02	14.40 ± 0.02
59562.65	+98.25	16.23 ± 0.03	15.15 ± 0.03	14.58 ± 0.02	14.42 ± 0.02
59567.56	+103.16	16.48 ± 0.11	15.33 ± 0.05	14.70 ± 0.04	14.46 ± 0.02
59571.60	+107.20	16.62 ± 0.03	15.34 ± 0.02	14.71 ± 0.03	14.50 ± 0.02
59581.58	+117.18	17.05 ± 0.02	15.67 ± 0.02	14.94 ± 0.02	14.70 ± 0.03
59583.48	+119.08	17.10 ± 0.02	15.79 ± 0.02	15.01 ± 0.02	14.77 ± 0.02
59585.56	+121.16	17.28 ± 0.02	15.87 ± 0.03	15.09 ± 0.03	14.86 ± 0.02
59587.53	+123.13	17.38 ± 0.02	15.98 ± 0.02	15.14 ± 0.02	14.89 ± 0.02
59590.41	+126.01	17.44 ± 0.07	16.04 ± 0.05	15.19 ± 0.02	14.98 ± 0.02
59591.55	+127.15	17.62 ± 0.03	16.14 ± 0.02	15.33 ± 0.02	15.05 ± 0.02
59594.52	+130.12	17.80 ± 0.03	16.34 ± 0.02	15.43 ± 0.02	15.18 ± 0.02
59596.52	+132.12	17.71 ± 0.06	16.44 ± 0.04	15.44 ± 0.02	15.24 ± 0.03
59606.47	+142.07	18.35 ± 0.03	16.85 ± 0.02	15.82 ± 0.02	15.57 ± 0.02
59607.46	+143.06	18.15 ± 0.04	16.82 ± 0.02	15.82 ± 0.02	15.58 ± 0.02
59609.46	+145.06	18.27 ± 0.16	–	15.90 ± 0.02	15.62 ± 0.03
59612.48	+148.08	18.33 ± 0.05	16.94 ± 0.03	15.87 ± 0.02	15.65 ± 0.02
59626.49	+162.09	–	–	–	15.78 ± 0.02
59628.44	+164.04	18.37 ± 0.11	17.16 ± 0.03	15.97 ± 0.02	15.85 ± 0.03
59641.44	+177.04	18.32 ± 0.21	17.26 ± 0.03	16.05 ± 0.02	15.90 ± 0.02
59788.80	+324.40	–	19.01 ± 0.11	17.52 ± 0.02	–
59792.79	+328.39	–	18.91 ± 0.04	17.54 ± 0.02	17.52 ± 0.02
59819.82	+355.42	–	–	17.87 ± 0.02	–
59820.78	+356.38	–	19.19 ± 0.11	–	–
59851.71	+387.31	–	19.51 ± 0.04	18.34 ± 0.02	18.22 ± 0.02
59865.72	+401.32	20.77 ± 0.39	19.65 ± 0.07	18.68 ± 0.05	18.52 ± 0.08
59877.74	+413.34	–	–	18.75 ± 0.02	18.62 ± 0.04
59885.58	+421.18	20.99 ± 0.48	19.94 ± 0.09	18.91 ± 0.04	18.73 ± 0.03
59904.58	+440.18	–	20.05 ± 0.06	19.19 ± 0.03	19.03 ± 0.03
59928.57	+464.17	–	20.18 ± 0.13	19.57 ± 0.03	19.47 ± 0.05

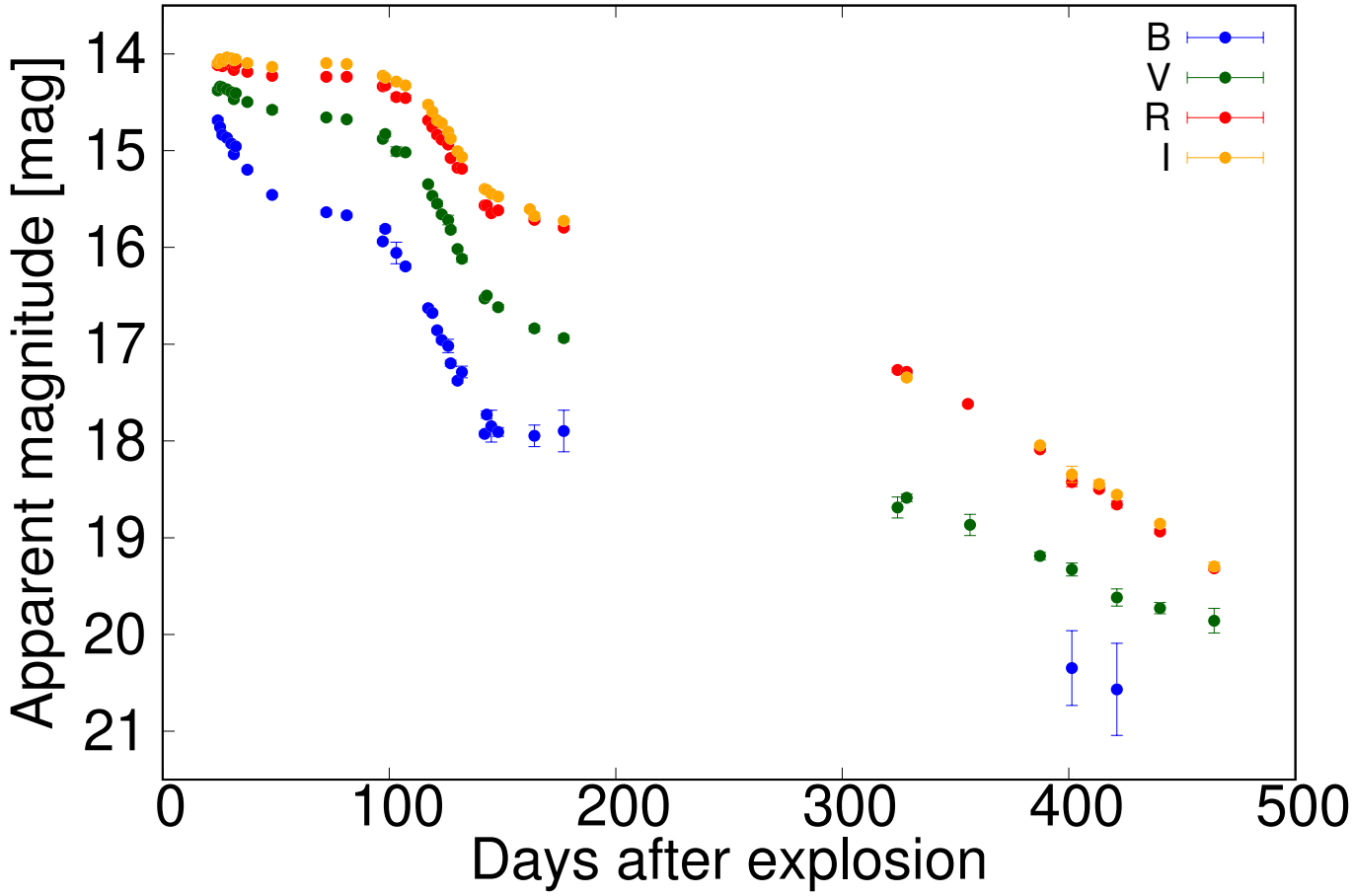

Fig. B.1. Light curves of SN 2021yja in the optical (*BVRI*) bands. The magnitudes have been corrected for a reddening of $E(B-V) = 0.104$

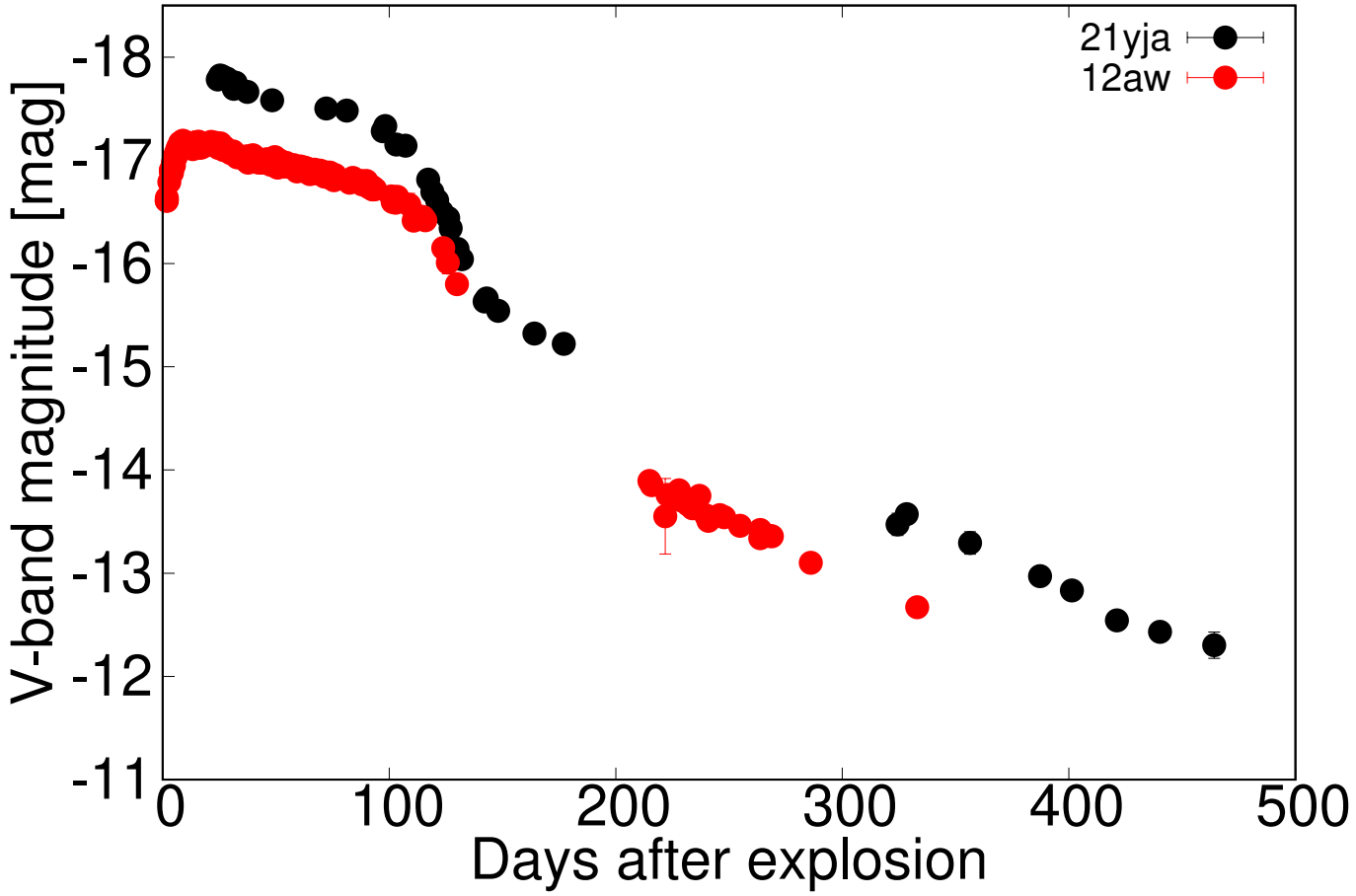

Fig. B.2. Time evolution of the V-band absolute magnitudes of SNe 2021yja and 2012aw. The data of SN 2012aw were taken from Munari et al. (2013), Bose et al. (2013), Dall'Ora et al. (2014), Brown et al. (2014). The V-band extinction for SN 2012aw is assumed to be $A_V = 0.23$ mag (Bose et al. 2013).

Appendix C: Spectroscopy

In addition to the spectra obtained from the spectropolarimetric observations with the FORS2/VLT (see Section 2), we obtained optical spectra of SN 2021yja using the Kyoto Okayama Optical Low-dispersion Spectrograph with optical-fiber Integral Field Unit (KOOLS-IFU; Matsubayashi et al. 2019) mounted on the Seimei telescope (Kurita et al. 2020) at the Okayama Observatory of Kyoto University and the Alhambra Faint Object Spectrograph and Camera (ALFOSC)[3] mounted on the 2.56-m Nordic Optical Telescope (NOT)[4] at the Roque de los Muchachos Observatory. The log of spectroscopic observations are provided in Table C.1.

For the KOOLS-IFU/Seimei, we used the VPH-blue grism, giving a wavelength coverage of 4100-8900 Å and a spectral resolution of $R = \lambda/\Delta\lambda \sim 500$. The data reduction was performed following the standard procedures that are developed for KOOLS-IFU data[5], using the IRAF. For the ALFOSC/NOT, we used Grism 4, giving a wavelength coverage of 3200-9600 Å and a spectral resolution of $\sim$ 360. The spectrum was reduced with the alfoscgui pipeline[6]. The procedures include overscan, bias, and flat-field corrections, as well as removing cosmic-ray artefacts. Extraction of a one-dimensional spectrum and sky subtraction were performed. Wavelength calibration was performed by comparison with arc lamps. The spectra were flux-calibrated against a sensitivity function derived from a standard star observed on the same night. The reduced spectra are shown in Figures C.1 and C.2.

Table C.1. Log of the spectroscopic observations of SN 2021yja.

Date (UT)	MJD (days)	Phase (days)	Days from explosion (days)	Exp. time (seconds)	Instrument/Telescope
2021 – 09 – 09.75	59466.75	–123.82	+2.35	300 × 3	KOOLS-IFU/Seimei
2021 – 09 – 15.79	59472.79	–117.78	+8.39	600 × 3	KOOLS-IFU/Seimei
2021 – 09 – 18.76	59475.76	–114.81	+11.36	300 × 3	KOOLS-IFU/Seimei
2021 – 09 – 19.76	59476.76	–113.81	+12.36	600 × 3	KOOLS-IFU/Seimei
2021 – 09 – 29.78	59486.78	–103.79	+22.38	900 × 3	KOOLS-IFU/Seimei
2021 – 10 – 02.24	59489.24	–101.33	+24.84	300 × 4	FORS2/VLT
2021 – 10 – 05.78	59492.78	–97.79	+28.38	300 × 3	KOOLS-IFU/Seimei
2021 – 11 – 11.26	59529.26	–61.31	+64.86	300 × 4	FORS2/VLT
2021 – 11 – 14.60	59532.60	–59.97	+68.20	600 × 3	KOOLS-IFU/Seimei
2021 – 12 – 03.09	59551.09	–39.48	+86.69	300 × 4	FORS2/VLT
2021 – 12 – 30.51	59578.51	–12.06	+114.11	1200 × 2	KOOLS-IFU/Seimei
2022 – 01 – 06.10	59585.10	–5.47	+120.70	300 × 4	FORS2/VLT
2022 – 01 – 10.47	59589.47	–1.1	+125.07	1200 × 1	KOOLS-IFU/Seimei
2022 – 02 – 10.39	59620.39	+29.82	+155.99	600 × 2	KOOLS-IFU/Seimei
2022 – 08 – 26.22	59817.22	+226.65	+352.82	1800 × 1	ALFOSC/NOT
2022 – 09 – 21.74	59842.74	+252.17	+378.34	900 × 1	KOOLS-IFU/Seimei
2022 – 10 – 18.67	59870.67	+280.10	+406.27	900 × 3	KOOLS-IFU/Seimei

[3] https://www.not.iac.es/instruments/alfosc/
[4] https://www.not.iac.es/
[5] http://www.o.kwasan.kyoto-u.ac.jp/inst/p-kools/reduction-201806/index.html
[6] FOSCGUI is a graphical user interface aimed at extracting SN spectroscopy and photometry obtained with FOSC-like instruments. It was developed by E. Cappellaro. A package description can be found at https://sngroup.oapd.inaf.it/foscgui.html

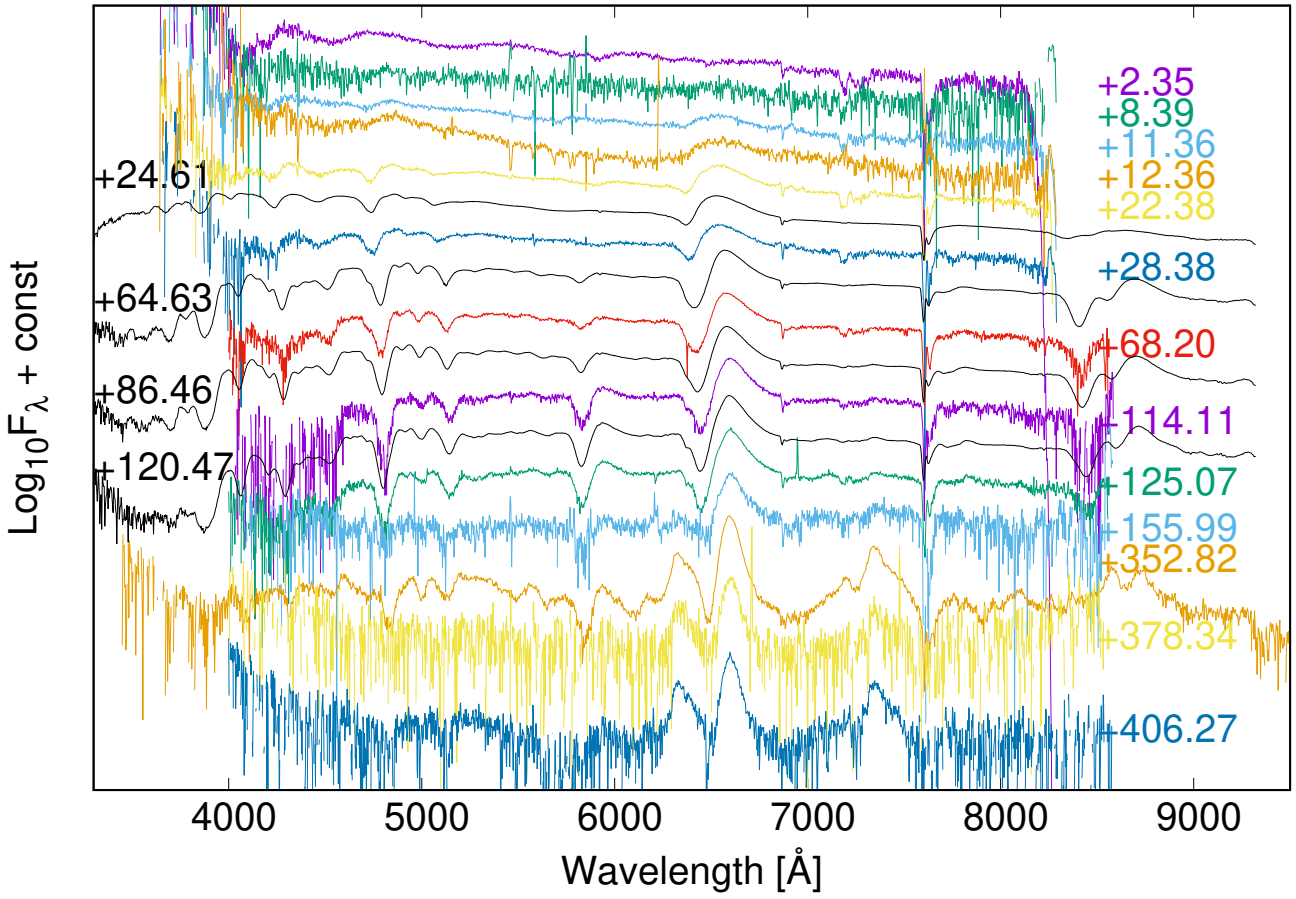

Fig. C.1. Spectral evolution of SN 2021yja. The numbers show days from the explosion.

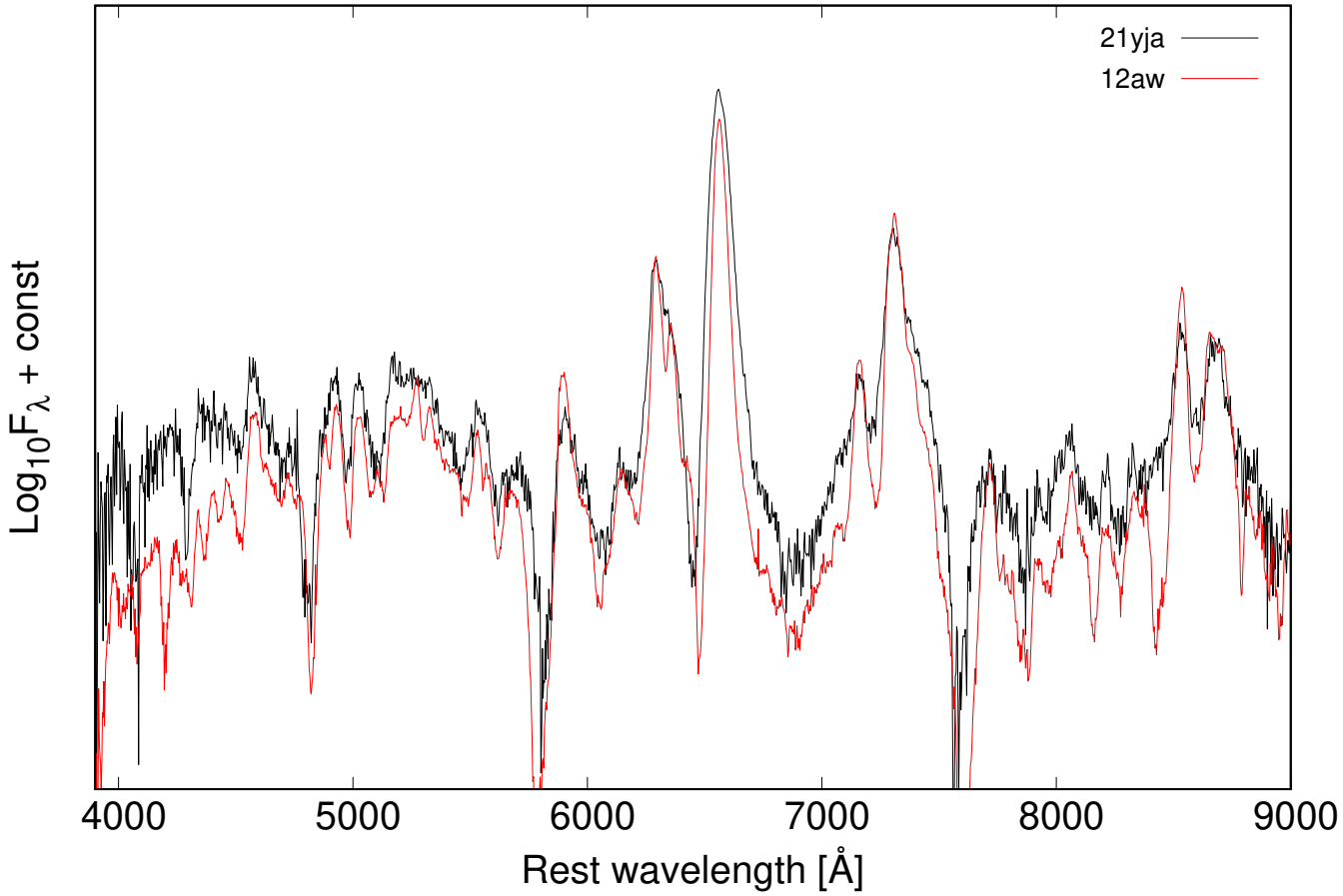

Fig. C.2. Same as Figure 4, but for the full wavelength range.